Electronic Supplementary Material (ESI) for Inorganic Chemistry Frontiers.

Supporting Information

Electronic metal-support interactions via Ni defect-induced Ru-modified Ni-CeO_2 for enhanced hydrogen oxidation activity

Shuqing Zhou,[a] Yi Liu,[a] Lianrui Cheng,[a] Tayirjan Taylor Isimjan,[b,*] Jianniao Tian,[a,*] and Xiulin Yang[a,*]

[a]*Guangxi Key Laboratory of Low Carbon Energy Materials, School of Chemistry and Pharmaceutical Sciences, Guangxi Normal University, Guilin 541004, China, E-mail addresses:* birdtjn@sina.com (*J. Tian*), *xlyang@gxnu.edu.cn (X. Yang)*

[b]*Saudi Arabia Basic Industries Corporation (SABIC) at King Abdullah University of Science and Technology (KAUST), Thuwal 23955-6900, Saudi Arabia, E-mail addresses: isimjant@sabic.com (T.T. Isimjan)*

Experimental Section

Chemicals

All chemicals and reagents were utilized as purchased without any further purification. These included trimesic acid-1,3,5-Benzenetricarboxylic acid ($C_9H_6O_6$ (H_3BTC), ≥98%, Aladdin), cerium(III) nitrate hexahydrate ($Ce(NO_3)_3·6H_2O$, ≥99%, Aladdin), nickel (II) nitrate hexahydrate ($Ni(NO_3)_2·6H_2O$, ≥98 %, Aladdin), ruthenium trichloride ($RuCl_3·xH_2O$, ≥99%, ~40 wt.% Ru, Aladdin), commercial Pt/C (20 wt.% Pt), nafion solution (5 wt.%), N,N-Dimethylformamide (DMF) and potassium hydroxide (KOH, AR, ≥95%, Aladdin). The deionized water (18.25 MΩ cm^{-1}) from a water purification system (Ulupure) was used throughout the whole experiment.

Preparation of NiCe-MOF

Specifically, 0.325 g $Ce(NO_3)_3·6H_2O$ and 0.218 g $Ni(NO_3)_2·6H_2O$ were dissolved in 30 mL DMF. The solution was sonicated for 15 minutes and then 15 ml of DMF (containing 0.315 g of H_3BTC) was titrated. After remaining stirred for 30 minutes, the mixture was transferred to a 100 ml Teflon lined reactor and holding at 160 ºC for 24 hours. After cooling to room temperature, the product was centrifuged, washed three times with DMF, and dried overnight in an oven at 60 °C to yield NiCe-MOF. Except that $Ce(NO_3)_3·6H_2O$ or $Ni(NO_3)_2·6H_2O$ was not added in the preparation process, the syntheses of Ni-MOF and Ce-MOF were completely identical.

Preparation of Ni-CeO_2

Annealing of the NiCe-MOF precursor at 700 °C (650, 750 or 800 °C) for 2 hours in an Ar atmosphere at a heating rate of 5 °C min^{-1}. After cooling naturally, the prepared sample was

named Ni-CeO_2 (Ni-CeO_2-650, Ni-CeO_2-750 or Ni-CeO_2-800 °C). The Ni-MOF and Ce-MOF were annealed identically and labeled Ni and CeO_2, respectively.

Preparation of Ru/Ni-CeO_2

Generally, the synthesized Ni-CeO_2 (50 mg) was scattered in a mixture of deionized water/glycol (40 ml, 1:3 v/v) and agitated to produce a homogeneous solution. Then, an amount of 10 mg $RuCl_3$ (5 or 15 mg) was added to the above-mentioned suspension and reacted for 5 h at 120 °C in an oil bath. Afterwards, it was washed three times with deionized water and ethanol, and dried overnight in an oven at 60 °C to obtain Ru/Ni-CeO_2. The Ru content was 3.75 wt.%, confirmed by inductively coupled plasma (ICP-MS) measurements. For comparison, we obtained other samples labeled Ru/Ni and Ru/CeO_2 following the same line of approach.

Materials Characterization

Powder X-ray diffraction (XRD, Rigaku D/Max 2500V/PC, Japan, Cu Ka radiation over the 2θ range of 10-90^o) was measured to investigate the crystal structure and phase composition of samples. Scanning electron microscopy (SEM, FEI Quanta 200 FEG) and transmission electron microscopy (TEM, JEM-2100 F) were recorded to characterize the morphology and elemental distribution of the catalysts. The chemical state and electronic structure of the samples were analyzed by X-ray photoelectron spectroscopy (XPS, JPS-9010 Mg Kα). Metal contents in the catalysts were examined using inductively coupled plasma mass spectroscopy (ICP-MS, PerkinElmer corporation, FLexar-NexION300X). The specific BET surface area (Brunauer–Emmett–Teller) and pore size distribution of the samples were used to measure the specific surface area and pore size distribution, respectively. Raman spectra were obtained

using a Renishaw in Via with a visible laser (k = 532 nm).

Electrochemical Characterization

All the electrocatalytic measurements were performed in a standard three-electrode system by the CHI 760E (Shanghai, China) electrochemical analyzer. In this work, glassy carbon electrode (GCE, diameter: 5 mm, disk area: 0.196 cm^2) was chosen as the working electrode, graphite rod and saturated KCl-filled with Ag/AgCl were served as counter electrode and reference electrode, respectively. Electrochemical impedance spectroscopy (EIS) was measured using a multichannel potentiostat (Biologic VMP3) at the open circuit potential from 200 kHz to 10 mHz. All the measured potentials were converted relative to reversible hydrogen electrode (RHE) and *iR*-corrected by the resistance of the electrolyte according to the following equation: $E_{Ag/AgCl} + 0.197 + 0.059 \times pH - iR$.

Preparation of Catalytic Electrodes

To fabricate a thin-film working electrode, 2 mg of sample and 5 μL of nafion solution (5 wt.%), were ultrasonically dispersed in deionized water-isopropanol solution (volume ratio,1: 1) to form a homogeneous ink. Afterwards, 10 μL well-dispersed catalyst ink was suspended onto the pre-polished glassy carbon electrode, drying ink prior to measurement. The amount of Ru loading was 12.6 μg_{Ru} cm^{-2}, which was calculated by ICP-AES data.

Hydrogen Oxidation Reaction (HOR) Measurements

Before HOR measurements, the 0.1 KOH electrolyte was bubbled with UHP H_2 gas for 30 min to gain H_2-saturated 0.1 M KOH solution. Cyclic voltammetry (CV) curves were recorded between 0 V and 1.0 V vs. reversible hydrogen electrode (vs. RHE) in pre-made N_2-saturated 0.1 M KOH electrolyte until the stable curves were obtained. HOR polarization curves

were collected at a sweep rate of 10 mV s^{-1} ranging from -0.05 V to 0.5 V (vs. RHE) under 1600 revolutions per minute (rpm) of the rotating disk electrode (RDE) rotation rate. The stability was assessed by repeating the potential scan from 0 V to 1.0 V (vs. RHE) for 1000 cycles at the scanning rate of 100 mV s^{-1}. Chronoamperometric characterization was performed at 50 mV vs. RHE.

Koutecky-Levich equation was used to calculate the kinetic current density [1]:

$$\frac{1}{j_d} + \frac{1}{j_k} = \frac{1}{j}$$

Where j_d is the diffusion current density [mA cm^{-2}], j_k is the kinetic current density [mA cm^{-2}], and j is the measured current density [mA cm^{-2}].

Levich equation [2]:

$$j_d = 0.62nFD^{3/2}v^{-1/6}C_0\omega^{1/2} = BC_0\omega^{1/2}$$

In the formula, n, F, D correspond to the number of electrons transferred in the HOR, the Faraday constant (96485 C mol^{-1}) and H_2 diffusivity in the electrolytes (3.7×10^{-5} cm^2 s^{-1}), respectively. B is the Levich constant, C_0 is the solubility of H_2 (7.33×10^{-4} mol L^{-1}) and ω is the rotating speed.

Butler-Volmer equation [3]:

$$j_k = j_0 \left[e^{\eta \frac{\alpha F}{RT}} - e^{\eta \frac{-(1-\alpha)F}{RT}} \right]$$

Exchange current density (j_0), often used to evaluate the intrinsic activity of a catalyst, it could be evaluated from the Bulter-Volmer equation′s micro-polarization regions, where η, α is the overpotential and transfer coefficient respectively, R, T represent the gas constant (8.314 J mol^{-1} K^{-1}) and the testing temperature (303 K) respectively.

Mass activity (MA) was normalized by using j_k and the mass active metal dripped onto the

RDE [4].

$$\text{MA} = \frac{j_k}{M}$$

The specific activity (SA) was normalized by the electrochemically active surface area (ECSA) of active metals deposited on the RDE surface [5].

$$\text{SA} = \frac{j_k}{ECSA}$$

CO stripping voltammetry measurements was performed by holding the potential of working electrode at 0.1V (vs. RHE) for 10 min in the UHP CO to fully adsorb CO on the metal surface. Following, N_2 was bubbled for 40 min to completely remove residual CO in the electrolyte. CO stripping current was obtained by cycling between 0 V and 1.2 V (vs. RHE) at 0.02V s^{-1} without any extra CO. The 1st CV is the stripping of the monolayer CO, where the CO oxidation peak can be noticed. The 2nd CV represented the background [5].

$$\text{ECSA}_{\text{active metal}} = \frac{Q_{co}}{0.42\ mC\ cm^{-2} * M}$$

where Q_{CO} is the total charge of adsorbed CO oxidation, 0.42 mC cm^{-2} corresponds to monolayer CO adsorption and M represents the total loading of active metal on the working electrode.

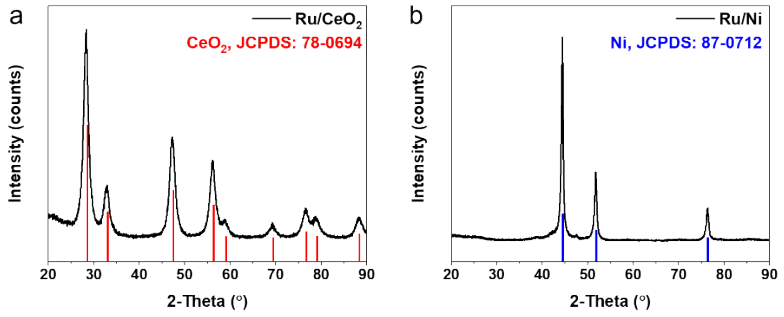

Fig. S1 XRD patterns of (a) Ru/CeO_2 and (b) Ru/Ni.

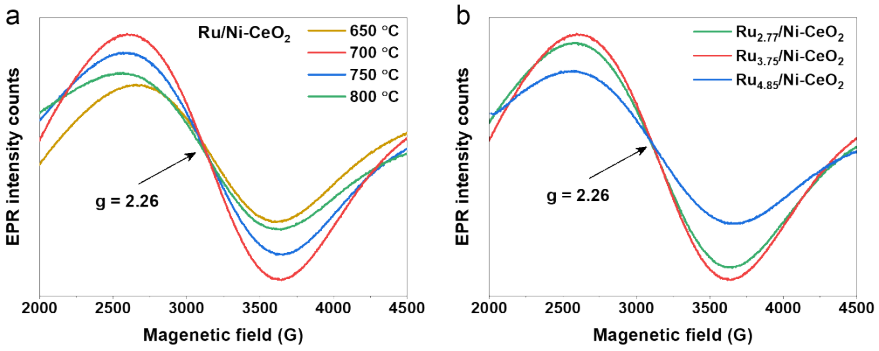

Fig. S2 EPR spectra of Ru/Ni-CeO_2 for (a) different calcination temperatures and (b) different Ru loading.

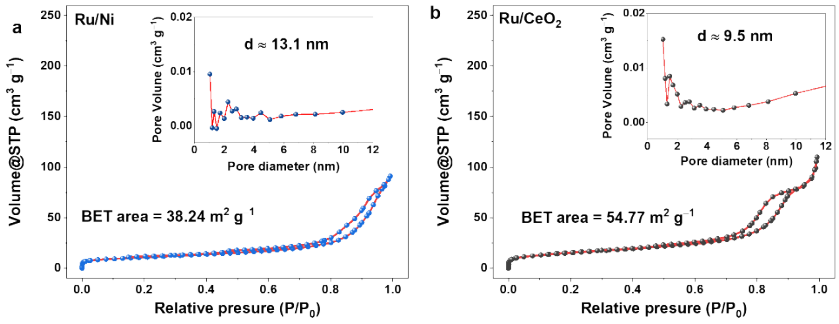

Fig. S3 N_2 adsorption-desorption isotherms with the corresponding pore size distribution of (a) Ru/Ni and (b) Ru/CeO_2.

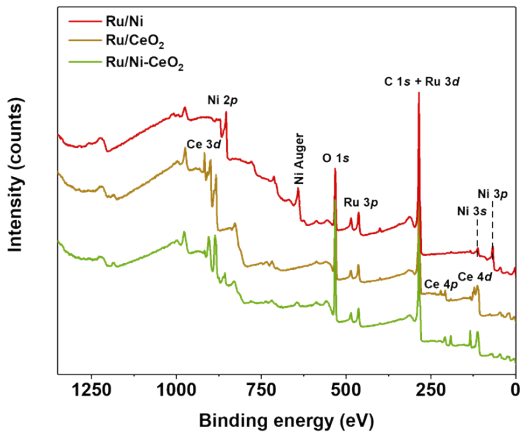

Fig. S4 XPS survey spectra of Ru/Ni-CeO_2

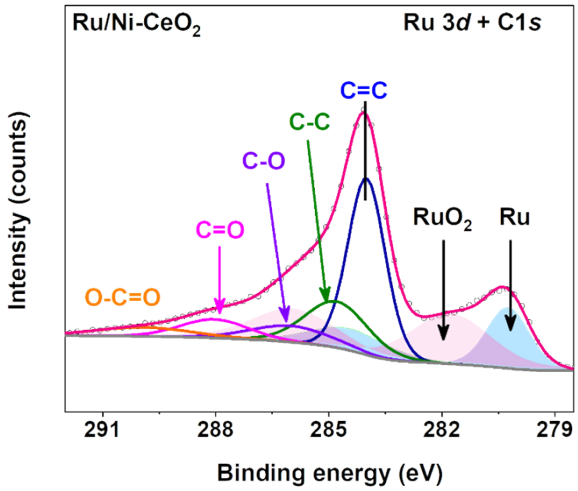

Fig. S5 High-resolution XPS spectrum of Ru 3*d* + C 1*s*.

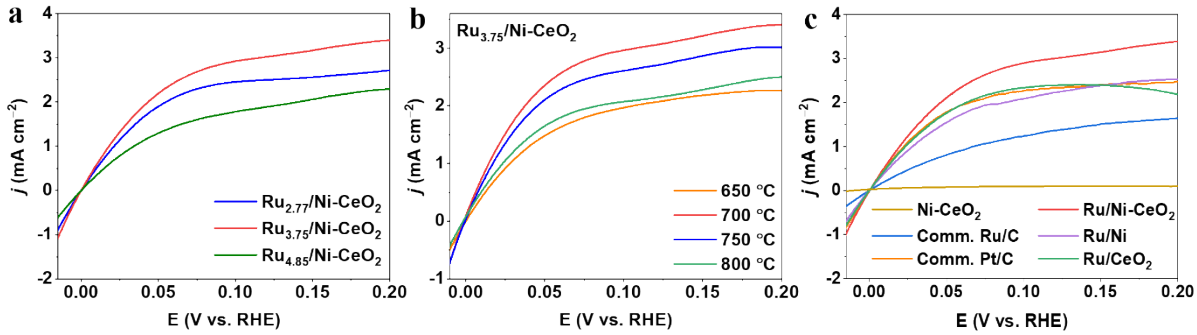

Fig. S6 HOR polarization curves without compensation of Ru/Ni-CeO_2 in H_2-saturated 0.1 M KOH at the rotating speed of 1600 rpm for (a) different calcination temperatures. (b) Different Ru loading. (c) Different of catalysts.

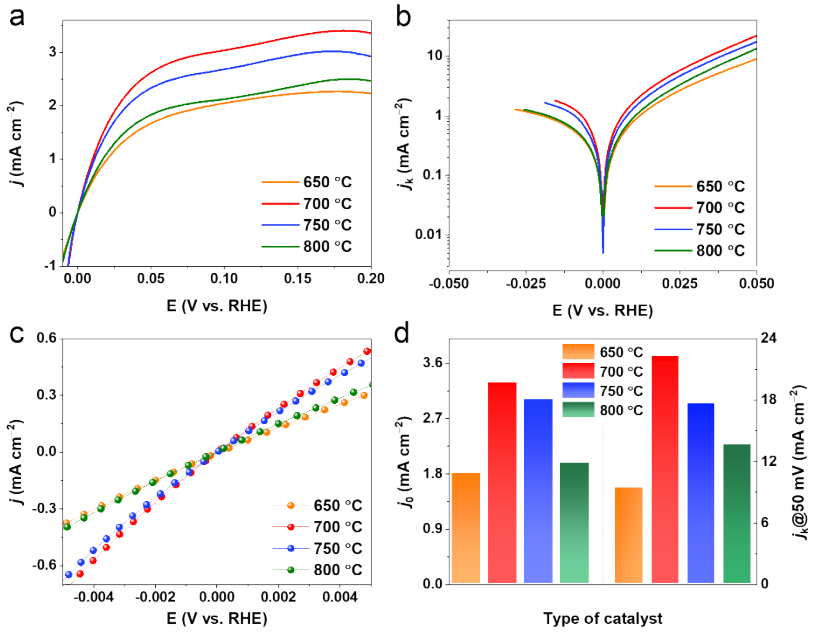

Fig. S7 (a) HOR polarization curves of Ru/Ni-CeO_2 in H_2-saturated 0.1 M KOH at the rotating speed of 1600 rpm for different calcination temperatures. (b) Tafel plots. (c) Linear fitting curves in micropolarization region. (d) Summarization of j_k and j_0 of Ru/Ni-CeO_2 at different calcination temperatures.

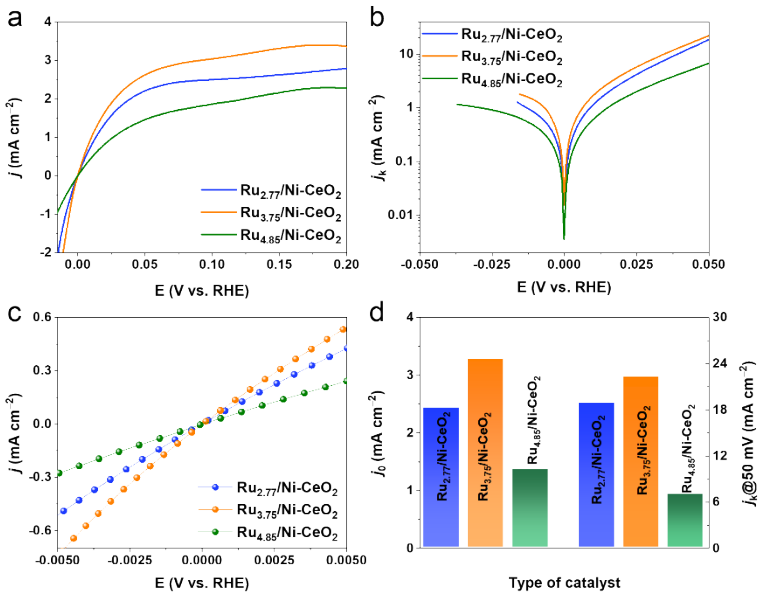

Fig. S8 (a) HOR polarization curves of Ru/Ni-CeO_2 in H_2-saturated 0.1 M KOH at the rotating speed of 1600 rpm for different Ru loading. (b) Tafel plots. (c) Linear fitting curves in micropolarization region. (d) Summarization of j_k and j_0 of Ru/Ni-CeO_2 at different Ru loading.

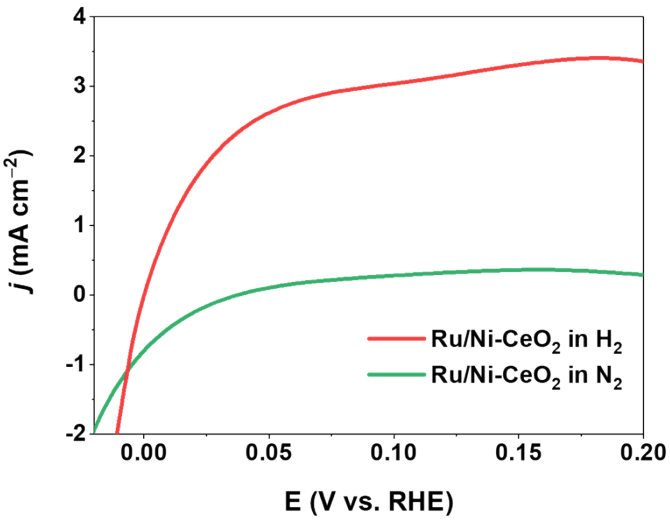

Fig. S9 Polarization curve of Ru/Ni-CeO_2 in N_2-saturated and H_2-saturated 0.1 M KOH at the rotating speed of 1600 rpm.

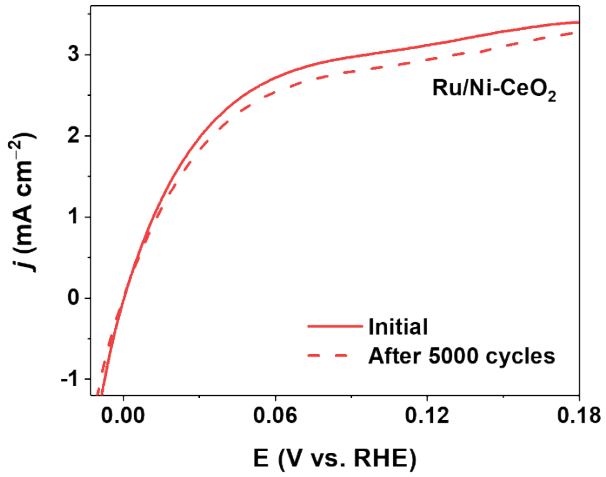

Fig. S10 HOR polarization curves of Ru/Ni-CeO_2 in H_2-saturated 0.1 M KOH before and after 5000 CVs.

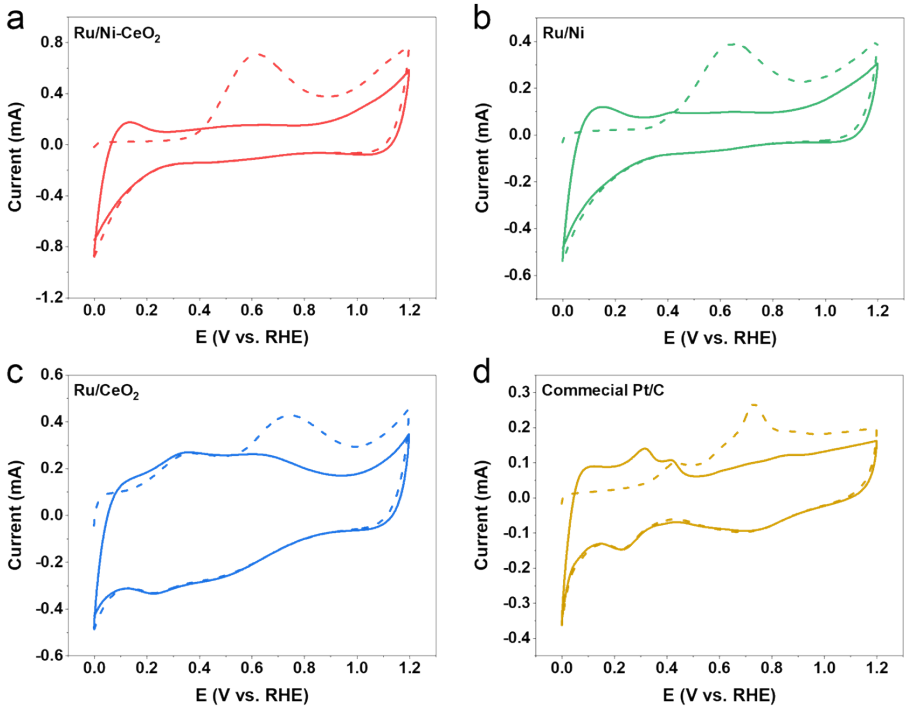

Fig. S11 CO stripping curves of (a) Ru/Ni-CeO_2, (b) Ru/Ni, (c) Ru/CeO_2, and (d) commercial Pt/C in CO-saturated 0.1 M KOH.

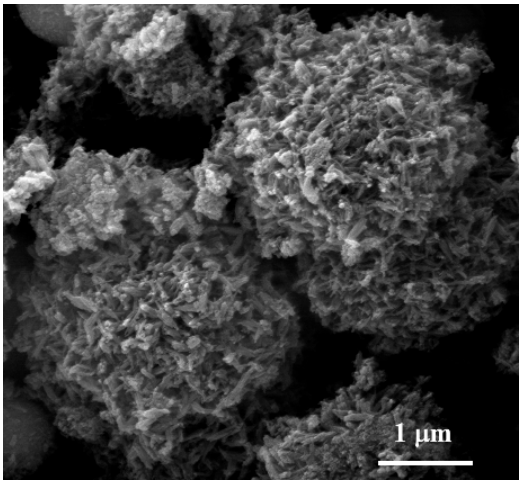

Fig. S12 SEM image of Ru/Ni-CeO_2 after 1000 cycles of cyclic voltammetry stability test for HOR.

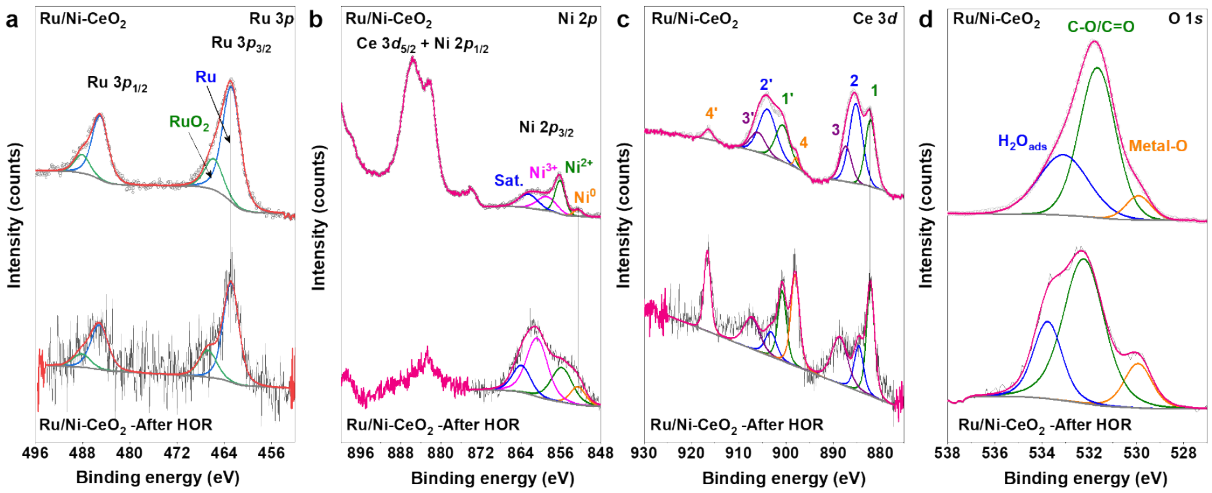

Fig. S13 High-resolution XPS spectra of (a) Ru 3*p*, (b) Ni 2*p*, (c) Ce 3*d*, and (d) O 1*s* after long-term stability test toward HOR.

Table S1. Inductively coupled plasma atomic emission spectroscopy (ICP-AES) of different materials

Catalyst	Ru (wt.%)
Ru/Ni	3.72
Ru/CeO_2	3.62
Ru_5/Ni-CeO_2	2.77
Ru_{10}/Ni-CeO_2	**3.75**
Ru_{15}/Ni-CeO_2	4.85

Note: In this process, about 2.0 mg samples were dissolved in aqua regia solution, and then diluted into 2.0 mg/L catalyst solution. Before ICP testing, the prepared solution was further diluted into about 200 μg/L catalyst solution. The standard solution of Ru was bought from commercial company and used directly.

Table S2. Summary of ECSA, MA, SA, j_k, and j_0 of different catalysts in this work

Catalysts	ECSA [$m^2\ g^{-1}$]	MA [mA μg^{-1}]	j_k [mA cm^{-2}] @=50mV	j_0 [mA cm^{-2}]	SA [mA cm^{-2}]
Ru/Ni-CeO_2	**62.1**	**1.93**	**22.2**	**3.27**	0.32
Ru/CeO_2	19.2	0.75	8.3	2.07	0.37
Ru/Ni	30.5	0.47	5.4	1.65	0.16
Pt/C	35.7	0.22	7.8	2.23	0.054

Note: MA: mass activity at 50 mV. SA: specific activity. j_k: kinetic current density at 50 mV. j_0: exchange current density from the micro-polarization region (-5 to 5 mV) by linear fitting through the Butler-Volmer equation.

Table S3 Electrochemical performances of Ru/Ni-CeO_2 on HOR compared with other catalysts

Catalysts	Electrolyte	MA@ 50mV [mA μg^{-1}_{metal}]	Reference
Ru/Ni-CeO_2	**0.1 M KOH**	**1.93**	**This work**
Ru-Ru_2P/C	0.1 M KOH	1.26	[1]
RuFe	0.1 M KOH	0.93	[2]
Mo-Ru-1/C	0.1 M KOH	1.73	[3]
Ga-Ru/C	0.1 M KOH	0.59	[4]
di-Ru/Ni	0.1 M KOH	1.79	[5]
MoO_x-Ru hcp	0.1 M KOH	1.16	[6]
Ru-Ir/C-20	0.1 M KOH	0.61	[7]
Mo-Ru-3/C	0.1 M KOH	1.25	[3]
Ru/XC	0.1 M KOH	0.374	[8]
Ru/PEI-XC	0.1 M KOH	0.423	[8]
O-RuNi@C	0.1 M KOH	0.601	[9]
Ru/RuO_2-180	0.1 M KOH	0.92	[10]
$Ir_1Pd_1Ru_8$	0.1 M KOH	1.26	[11]
$Ru_{0.20}Pd_{0.80}$/C	0.1 M KOH	1.02	[12]

Ir/Ni-NiO/CNT	0.1 M KOH	1.56	[13]
hcp Ru NAs	0.1 M KOH	0.74	[14]
Sn-Ru/C	0.1 M KOH	1.79	[4]
IO-Ru-TiO_2/C	0.1 M KOH	0.907	[15]
$Pt_{0.25}Ru_{0.75}$/NC	0.1 M KOH	1.65	[16]
$Pb_{1.04}$-$Ru_{92}Cu_8$/C	0.1 M KOH	1.10	[17]

References

1 L. Su, Y. Jin, D. Gong, X. Ge, W. Zhang, X. Fan, W. Luo, The Role of Discrepant Reactive Intermediates on Ru-Ru_2P Heterostructure for pH-Universal Hydrogen Oxidation Reaction, *Angew. Chem. Int. Ed.*, 2022, **62**, e202215585.

2 Y. Li, C. Yang, C. Ge, N. Yao, J. Yin, W. Jiang, H. Cong, G. Cheng, W. Luo, L. Zhuang, Electronic Modulation of Ru Nanosheet by d-d Orbital Coupling for Enhanced Hydrogen Oxidation Reaction in Alkaline Electrolytes, *Small*, 2022, **18**, 2202404.

3 Y. Zhao, D. Wu, W. Luo, Correlating Alkaline Hydrogen Electrocatalysis and Hydroxide Binding Energies on Mo-Modified Ru Catalysts, *ACS Sustainable Chem. Eng.*, 2022, **10**, 1616-1623.

4 L. Wu, L. Su, Q. Liang, W. Zhang, Y. Men, W. Luo, Boosting Hydrogen Oxidation Kinetics by Promoting Interfacial Water Adsorption on d-p Hybridized Ru Catalysts, *ACS Catal.*, 2023, **13**, 4127-4133.

5 Y. Dong, Q. Sun, C. Zhan, J. Zhang, H. Yang, T. Cheng, Y. Xu, Z. Hu, C.W. Pao, H. Geng, X. Huang, Lattice and Surface Engineering of Ruthenium Nanostructures for Enhanced Hydrogen Oxidation Catalysis, *Adv. Funct. Mater.*, 2022, **33**, 2210328.

6 L. Li, C. Liu, S. Liu, J. Wang, J. Han, T.-S. Chan, Y. Li, Z. Hu, Q. Shao, Q. Zhang, X. Huang, Phase Engineering of a Ruthenium Nanostructure toward High-Performance Bifunctional Hydrogen Catalysis, *ACS Nano*, 2022, **16**, 14885-14894.

7 J. Ohyama, D. Kumada, A. Satsuma, Improved hydrogen oxidation reaction under alkaline conditions by ruthenium–iridium alloyed nanoparticles, *J. Mater. Chem. A*, 2016, **4**, 15980-15985.

8 J. Wang, J. Liu, B. Zhang, J. Gao, G. Liu, X. Cui, J.-X. Liu, L. Jiang, Amine-ligand modulated ruthenium nanoclusters as a superior bi-functional hydrogen electrocatalyst in alkaline media, *J. Mater. Chem. A*, 2021, **9**, 22934-22942.

9 X. Zhang, Z. Li, X. Sun, L. Wei, H. Niu, S. Chen, Q. Chen, C. Wang, F. Zheng, Regulating the Surface Electronic Structure of RuNi Alloys for Boosting Alkaline Hydrogen Oxidation Electrocatalysis, *ACS Mater. Lett.*, 2022, **4**, 2097-2105.

10 X. Zhang, L. Xia, G. Zhao, B. Zhang, Y. Chen, J. Chen, M. Gao, Y. Jiang, Y. Liu, H. Pan, W. Sun, Fast and Durable Alkaline Hydrogen Oxidation Reaction at the Electron-Deficient Ruthenium–Ruthenium Oxide Interface, *Adv. Mater.*, 2023, **35**, 2208821.

11 H. Wang, H.D. Abruña, IrPdRu/C as H2 Oxidation Catalysts for Alkaline Fuel Cells, *J. Am. Chem. Soc.*, 2017, **139**, 6807-6810.

12 S. St. John, R.W. Atkinson, R.R. Unocic, T.A. Zawodzinski, A.B. Papandrew, Ruthenium-Alloy

Electrocatalysts with Tunable Hydrogen Oxidation Kinetics in Alkaline Electrolyte, *J. Phys. Chem. C*, 2015, **119**, 13481-13487.

13 X. Ji, P. Chen, Y. Liu, Z. Ji, H. Zhou, C. Chen, X. Shen, X. Fu, G. Zhu, Ir/Ni–NiO/CNT composites as effective electrocatalysts for hydrogen oxidation, *J. Mater. Chem. A*, 2023, **11**, 5076-5082.

14 J. Zhang, M. Cao, X. Li, Y. Xu, W. Zhao, L. Chen, Y.C. Chang, C.W. Pao, Z. Hu, X. Huang, Kinetic-Modulated Crystal Phase of Ru for Hydrogen Oxidation, *Small*, 2023, **19**, 2207038.

15 J. Jiang, S. Tao, Q. He, J. Wang, Y. Zhou, Z. Xie, W. Ding, Z. Wei, Interphase-oxidized ruthenium metal with half-filled d-orbitals for hydrogen oxidation in an alkaline solution, *J. Mater. Chem. A*, 2020, **8**, 10168-10174.

16 Y. Cong, C. Chai, X. Zhao, B. Yi, Y. Song, Pt0.25Ru0.75/N-C as Highly Active and Durable Electrocatalysts toward Alkaline Hydrogen Oxidation Reaction, *Adv. Mater. Interfaces*, 2020, **7**, 2000310.

17 Y. Dong, Z. Zhang, W. Yan, X. Hu, C. Zhan, Y. Xu, X. Huang, Pb-Modified Ultrathin RuCu Nanoflowers for Active, Stable, and CO-resistant Alkaline Electrocatalytic Hydrogen Oxidation, *Angew. Chem. Int. Ed.*, 2023, **62**, e202311722.